# Stable Jets of Viscoelastic Fluids and Self-Assembled Cylindrical Capsules by Hydrodynamic Focusing

K. V. Edmond,[†] A. B. Schofield,[‡] Manuel Marquez,[§] J. P. Rothstein,[||] and A. D. Dinsmore*,[†]

*Department of Physics, University of Massachusetts, Hasbrouck Lab, 666 North Pleasant Street, Amherst, Massachusetts 01003, School of Physics, University of Edinburgh, Edinburgh, EH9 3JZ, U.K., INEST Group, Philip Morris USA Research Center, 4201 Commerce Road, Richmond, Virginia 23234, and Department of Mechanical and Industrial Engineering, University of Massachusetts, Gunness Lab, 160 Governors Drive, Amherst, Massachusetts 01003*

*Received May 26, 2006. In Final Form: July 31, 2006*

We demonstrate formation of long-lived cylindrical jets of a viscoelastic fluid using hydrodynamic focusing. A solution of polyacrylamide in water is driven coaxially with immiscible oil and subjected to strong extensional flow. At high flow rates, the aqueous phase forms jets that are 4−90 $\mu$m in diameter and several centimeters long. The liquid surfaces of these jets are then used as templates for assembly of microspheres into novel rigid and hollow cylinders.

Emulsions are common in a host of products and processes within the food, pharmaceutical, and chemical industries. The surfaces of dispersed droplets are also used commonly for purification[1−3] and as templates for assembly of lipids[4] or colloidal particles for novel materials.[5−18] In recent years, a number of studies have investigated the use of flows developed within microfluidic devices, which offer precise control of drop size, shape, and polydispersity.[19−23] For example, monodisperse water droplets in oil were created using a planar microfluidic device in which a water phase and two surrounding oil phases were focused through a narrow orifice, which created a strong extensional flow and stretched the water into a narrow jet.[20] As the length of such jets exceeds the circumference, they become unstable against breakup into droplets.[24,25] In the small Ohnesorge number regime, $Oh = \eta/\sqrt{\rho\sigma R} \ll 1$, this breakup is resisted by inertia; the characteristic time for breakup of water jets in oil is approximately the inertio-capillary or Rayleigh time scale, $\tau_R = (\rho R/\sigma)^{1/2} \approx 10^{-5}$ s. Here $\sigma$ is the surface tension of the oil−water interface, $R$ is the jet's radius, $\rho$ is the mass density of the fluid, and $\eta$ is its shear viscosity. During this time the jet typically travels a relatively short distance; thus, droplets are formed by steady dripping.[22,26−28] Stabilizing the cylindrical jets, however, is of great practical utility in spray applications and materials preparation,[17] where hollow cylindrical capsules are desired. Methods to stabilize fluid jets include application of body forces, such as from an electric field.[7,29−31] The presence of a strong extensional flow has also been shown to stabilize jets and drops of Newtonian fluids.[32,33] Recent studies have also shown that hydrodynamic confinement can dramatically slow the break-up of liquid jets when the radius of the jet approaches the radius of the confining tube.[34−36]

Additionally, the viscoelasticity of the interior phase can forestall the break-up of laminar capillary jets.[37] For these fluids

* To whom correspondence should be addressed.
[†] Department of Physics, University of Massachusetts.
[‡] University of Edinburgh.
[§] Philip Morris USA Research Center.
[||] Department of Mechanical and Industrial Engineering, University of Massachusetts.

(1) Hamouda, T.; Myc, A.; Donovan, B.; Shih, A. Y.; Reuter, J. D.; Baker, J. R. *Microbiol. Res.* **2001**, *156*, 1−7.
(2) Gaudin, A. M. *Flotation*; McGraw-Hill: New York, 1957.
(3) Bhargava, A.; Francis, A. V.; Biswas, A. K. *J. Colloid Interface Sci.* **1978**, *64*, 214−227.
(4) Pautot, S.; Frisken, B. J.; Weitz, D. A. *Proc. Natl. Acad. Sci. U.S.A.* **2003**, *100*, 10718−10721.
(5) Velev, O. D.; Nagayama, K. *Langmuir* **1997**, *13*, 1856−1859.
(6) Dinsmore, A. D.; Hsu, M. F.; Nikolaides, M. G.; Marquez, M.; Bausch, A. R.; Weitz, D. A. *Science* **2002**, *298*, 1006.
(7) Loscertales, I. G.; Barrero, A.; Guerrero, I.; Cortijo, R.; Marquez, M.; Ganan-Calvo, A. M. *Science* **2002**, *295*, 1695−1698.
(8) Lin, Y.; Skaff, H.; Emrick, T. S.; Dinsmore, A. D.; Russell, T. P. *Science* **2003**, *299*, 226.
(9) Croll, L. M.; Stover, H. D. H. *Langmuir* **2003**, *19*, 5918.
(10) Wang, H.; Hobbie, E. K. *Langmuir* **2003**, *19*, 3091−3093.
(11) Reincke, T.; Hickey, S. G.; Kegel, W. K.; Vanmaekelbergh, D. *Angew. Chem., Int. Ed.* **2004**, *43*, 458−462.
(12) Duan, H.; Wang, D.; Kurth, D. G.; Mohwald, H. *Angew. Chem., Int. Ed.* **2004**, *43*, 5639.
(13) Stone, D. A.; Goldstein, R. E. *Proc. Natl. Acad. Sci U.S.A.* **2004**, *101*, 11537.
(14) Noble, P. F.; Cayre, O. J.; Alargova, R. G.; Velev, O. D.; Paunov, V. N. *J. Am. Chem. Soc.* **2004**, *126*, 8092−8093.
(15) Panhuis, M. I. H.; Paunov, V. N. *Chem. Commun.* **2005**, 1726−1728.
(16) Subramaniam, A. B.; Abkarian, M.; Stone, H. A. *Nat. Mater.* **2005**, *4*, 553−556.
(17) Stone, D. A.; Lewellyn, B.; Baygents, J. C.; Goldstein, R. E. *Langmuir* **2005**, *21*, 10916.
(18) Zeng, C.; Bissig, H.; Dinsmore, A. D. *Solid State Commun.*, in press.
(19) Thorsen, T.; Roberts, R. W.; Arnold, F. H.; Quake, S. R. *Phys. Rev. Lett.* **2001**, *86*, 4163−4166.
(20) Anna, S. L.; Bontoux, N.; Stone, H. A. *Appl. Phys. Lett.* **2003**, *82*, 364.
(21) Link, D. R.; Anna, S. L.; Weitz, D. A.; Stone, H. A. *Phys. Rev. Lett.* **2004**, *92*.
(22) Utada, A. S.; Lorenceau, E.; Link, D. R.; Kaplan, P. D.; Stone, H. A.; Weitz, D. A. *Science* **2005**, *308*, 537−541.
(23) Dendukuri, D.; Tsoi, K.; Hatton, T. A.; Doyle, P. S. *Langmuir* **2005**, *21*, 2113-2116.
(24) Rayleigh, L. *Proc. London Math. Soc.* **1879**, *10*, 4−13.
(25) Stone, H. A. *Annu. Rev. Fluid Mech.* **1994**, *26*, 65.
(26) Powers, T. R.; Goldstein, R. E. *Phys. Rev. Lett.* **1997**, *78*, 2555.
(27) Clanet, C.; Lasheras, J. C. *J. Fluid Mech.* **1999**, *383*, 307−326.
(28) Ambravaneswaran, B.; Subramani, H. J.; Phillips, S. D.; Basaran, O. A. *Phys. Rev. Lett.* **2004**, *93*.
(29) Sankaran, S.; Saville, D. A. *Phys. Fluids A* **1993**, *5*, 1081.
(30) Sanders, E. H.; Kloefkorn, R.; Bowlin, G. L.; Simpson, D. G.; Wnek, G. E. *Macromolecules* **2003**, *36*, 3803.
(31) Chen, X. P.; Jia, L. B.; Yin, X. Z.; Cheng, J. S.; Lu, J. *Phys. Fluids* **2005**, *17*.
(32) Taylor, G. I. *Proc. R. Soc. London A: Math. Phys. Sci* **1934**, *146*, 501.
(33) Tomotika, S. *Proc. R. Soc. London A: Math. Phys. Sci* **1936**, *153*, 0302−0318.
(34) Son, Y.; Martys, N. S.; Hagedorn, J. G.; Migler, K. B. *Macromolecules* **2003**, *36*, 5825−5833.
(35) Hagedorn, J. G.; Martys, N. S.; Douglas, J. F. *Phys. Rev. E* **2004**, *69*, 056312.
(36) Migler, K. B. *Phys. Rev. Lett.* **2001**, *86*, 1023−1026.
(37) Mun, R. P.; Byars, J. A.; Boger, D. V. *J. Non-Newtonian Fluid Mech.* **1998**, *74*, 285−297.

10.1021/la0614987 CCC: $33.50 
Published on Web 08/30/2006

the Ohnesorge number is typically large, $Oh \gg 1$, the breakup of the jet is resisted by the fluid viscosity, and the characteristic time scale for breakup is the visco-capillary time scale $\tau_v = \eta R/\sigma$. For a viscoelastic material, elasticity becomes important when the characteristic viscoelastic time scale, $\lambda$, approaches the characteristic time scale of the flow. In other words, when the Deborah number based on the extension rate, $\dot{\epsilon}$, developed within the jet becomes greater than 1 ($De = \lambda\dot{\epsilon} > 1$). For these viscoelastic fluids, it is the extensional viscosity $\eta_E$ and not the shear viscosity that resists the breakup of the fluid jet. The characteristic time for jet breakup is given by the viscoelastic-capillary time scale $\tau_E = \eta_E R/\sigma$.[38] For polymer solutions, the extensional viscosity can increase by several orders of magnitude as the extension rate and the accumulated strain are increased (the Trouton ratio $Tr \equiv \eta_E/\eta > 1000$).[39−41] Consequently, strain hardening has been shown to delay the breakup of viscoelastic jets by dramatically increasing the viscoelastic-capillary time scale.[37,42] If the viscoelastic capillary time scale is significantly larger than the residence time of the fluid in the flow focusing region, $\tau_E \gg \tau_{res}$, then continuous fluid jets rather than periodically dripping droplets will be formed.

In this article, we experimentally investigate the microfluidic flow focusing of an aqueous-phase coaxial with an immiscible oil phase. We demonstrate that using a viscoelastic polymer solution for the inner (aqueous) phase increases both the range of flow rates for which coherent jets can be produced and the duration of time over which the jets remain coherent downstream of the orifice. We present a scaling analysis based on balancing the destabilizing capillary stress with extensional and shear stresses to predict the form of the flow stability diagram. The results of the scaling analysis are in qualitative agreement with our experimental data. We also show that the stabilized fluid jets live long enough that they can be used as templates for the assembly of microparticles at the interface between the aqueous and oil phases. The result is a collection of long, rigid, and hollow cylinders that may find applications in encapsulation, as ultra-low-weight fillers for tough materials, and for basic studies of the morphology of crumpled elastic cylinders. Moreover, the results may be relevant to the use of non-Newtonian fluids in microfluidic applications, such as materials fabrication and lab-on-a chip devices.[43−45]

The flow geometry is shown in Figure 1 along with an image of a stable jet. Upstream of the extensional flow region the aqueous phase was driven inside a glass capillary with an outer diameter of 375 $\mu$m and an interior chamber having either a 20-$\mu$m-diameter circular cross-section (as in Figure 1b) or a 100-$\mu$m-wide interior chamber with an approximately square cross-section (Polymicro Technologies, Phoenix, AZ). This capillary was secured inside a larger glass capillary with an inner diameter of 500 $\mu$m. Hexadecane ($\eta = 3.3$ mPa·s) was driven through the gap between the inner and outer capillaries. The oil and aqueous phases exited through a downstream capillary, which had a 100 $\mu$m wide, approximately square cross-section and a length of more than 2 cm. In the 650 $\mu$m long gap between the coaxial upstream and downstream capillaries hydrodynamic flow focusing produced a strong extensional flow within the aqueous phase. The extensional (gap) region was sealed with a glass cover slip to allow imaging with a video camera. The flow rate of each phase was controlled independently by separate syringe pumps that operate under constant flow-rate conditions.

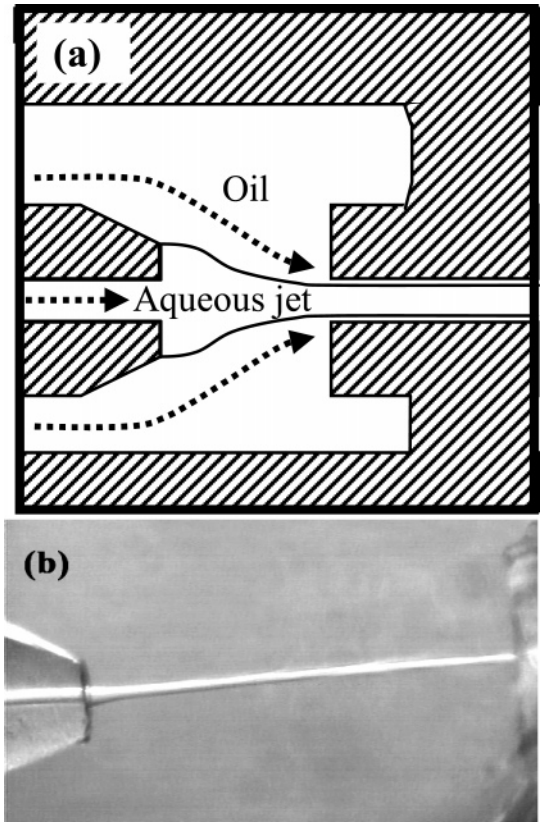


**Figure 1.** (a) Illustration of the flow apparatus in which an aqueous polymer phase undergoes coaxial flow with an oil phase (hexadecane). (b) Image of a jet of 1 wt % polyacrylamide (PAA) in water, coaxial with hexadecane. The jet is approximately 4 $\mu$m in diameter, and the inner diameter of the upstream capillary is 20 $\mu$m. The distance between the upstream and downstream capillaries is approximately 650 $\mu$m.

The viscoelastic interior fluid consisted of high molecular weight polyacrylamide (PAA) ($6 \times 10^6$ g/mol; Scientific Polymer Products, Inc., Ontario, NY) in Millipore-filtered water with no added salt or surfactant. We report flow data for polymer concentrations $c_p = 0$, 0.010, 0.10, and 1.0 wt %. The shear rheology of the fluids was characterized over a range of shear rates $\dot{\gamma}$ using a cone-and-plate rheometer (TA Instruments AR2000) and is presented in Figure 2. The measured zero-shear-rate viscosities were $\eta_0 = 0.002$, 0.008, and 2.9 Pa·s, and the relaxation times were 0.03, 0.04, and 0.2 s, respectively, for solutions with $c_p = 0.010$, 0.10, and 1.0 wt %. At the shear rates observed in our experiment (up to $10^4$ s$^{-1}$), the measured shear-rate-dependent viscosity $\eta(\dot{\gamma})$ approached that of water ($\eta = 0.001$ Pa·s). Polyacrylamide solutions also exhibit a large extensional viscosity $\eta_E$, which increases with the extension rate and accumulated strain;[46] we return to this point below.

Experimentation with different flow rates of oil and water revealed a set of flow rates $Q$ that separate long-lived coherent jets from periodic droplet production. The flow stability diagram (Figure 3) was obtained by setting the volume flow rates of the oil and aqueous phases ($Q_{oil}$ and $Q_{aq}$, respectively, in m$^3$/s) and using a video camera to observe the oil−water interface in the gap and the downstream capillary. All of the viscoelastic jets

(38) Fontelos, M. A.; Li, J. *J. Non-Newtonian Fluid Mech.* **2004**, *118*, 1−16.
(39) McKinley, G. H. In *Rheology Reviews*; Binding, D. M., Walters, K., Eds.; British Society of Rheology: Aberystwyth, Wales, UK, 2005; pp 1−48.
(40) McKinley, G. H.; Sridhar, T. *Annu. Rev. Fluid Mech.* **2002**, *34*, 375−415.
(41) Rothstein, J. P. *J. Rheol.* **2003**, *47*, 1227.
(42) Renardy, M. *J. Non-Newtonian Fluid Mech.* **1995**, *59*, 267−282.
(43) Groisman, A.; Enzelberger, M.; Quake, S. R. *Science* **2003**, *300*, 955−958.
(44) Stone, H. A.; Stroock, A. D.; Ajdari, A. *Annu. Rev. Fluid Mech.* **2004**, *36*, 381−411.
(45) Quake, S. R.; Scherer, A. *Science* **2000**, *290*, 1536−1540.
(46) Stelter, M.; Brenn, G.; Yarin, A. L.; Singh, R. P.; Durst, F. *J. Rheol.* **2000**, *44*, 595−616.

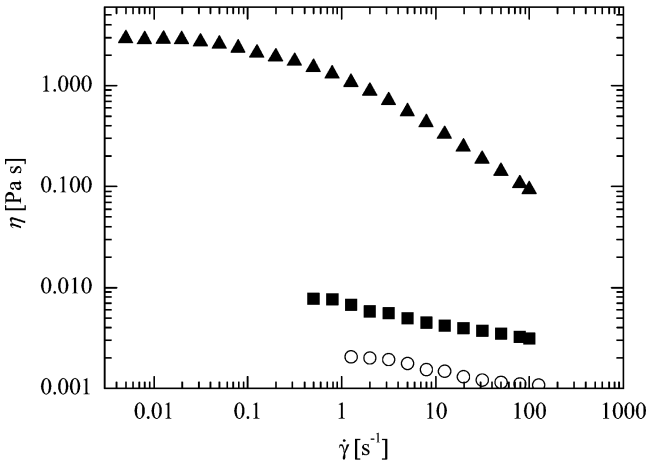


**Figure 2.** Measured steady shear viscosity, $\eta$, of aqueous polyacrylamide (PAA) solutions. Data points correspond to 0.01 (○), 0.1 (■), and 1.0 wt % PAA in water (▲).

persisted along the entire observable length of the downstream capillary, which corresponds to a minimum jet lifetime of 0.05−5 s. All of the results described here reflect the steady-state morphology of the aqueous phase. To determine the critical (minimum) flow rate for the fluid jets, $Q_{oil}$ and $Q_{aq}$ were first set well within the jetting region and then one of them was decreased in small increments, waiting for the flow to stabilize between steps.

When using a viscoelastic polymer solution for the inner phase, we observed stable jets at flow rates between 10 and 100 times smaller than when using pure water as the inner phase. It is important to note that increases in the shear viscosity alone would not result in such dramatic changes in the stability diagram. For the 0.01 wt % solution, for example, the zero shear rate viscosity is $\eta = 0.002$Pa·s; therefore, one would expect that the stable jets would be observed at flow rates of one-half, not one-tenth, of the pure water case. In fact, at the shear rates obtained within the microcapillaries ($\dot{\gamma} \approx 10^4 s^{-1}$), Figure 2 shows that the shear viscosity $\eta$ of each solution tested shear thins to approximately the viscosity of water ($\eta(\dot{\gamma} = 10^4 s^{-1}) \approx 0.001$Pa·s). The elasticity of the fluids and hence the extensional rheology thus play a large role in stabilizing the fluid jets.

Increasing the concentration of the polymer and thus the elasticity of the aqueous phase further extended the region for which stable jets were observed. With a fixed ratio of $Q_{oil}/Q_{aq} = 10$, for example, the critical value of $Q_{aq}$ was reduced by approximately 50 times as $c_p$ was increased 100 fold (Figure 3a). When the data are plotted in terms of the capillary number of the aqueous phase, $Ca \equiv \eta U/\sigma$, they collapse reasonably well onto an apparent master curve (Figure 3b). Here, $\eta$ is the shear-rate-dependent shear viscosity of the aqueous phase—taken directly from shear rheology data—and $U = Q_{aq}/(\pi R_{aq,u}^2)$ is the average velocity of the aqueous phase in the upstream capillary, which has a radius of $R_{cap,u}$. The solid curve in Figure 3 shows the prediction of a scaling argument that includes both shear and extension flow components, as described below.

The jets were observed to taper continuously across the span of the gap as shown in Figures 1 and 4. The reduction in cross-section area indicates an increase in jet velocity: the aqueous phase accelerated and was stretched within the gap. As expected from conservation of mass, the minimum jet diameter decreased as $Q_{oil}$ increased. With a 100 $\mu$m diameter upstream capillary (as in Figure 4), the minimum jet diameter decreased from 80 to 30 $\mu$m as $Q_{oil}/Q_{aq}$ increased from 1.1 to 42. (For these capillaries, the range of jet diameters was limited by the flow rates provided

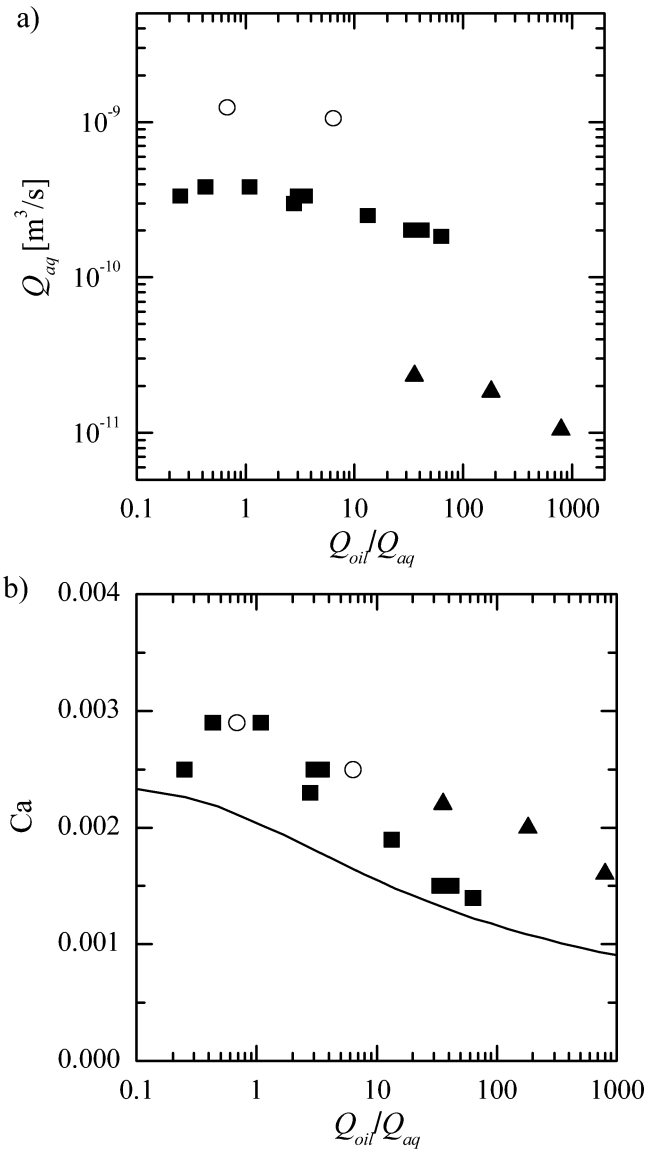


**Figure 3.** Measured flow stability diagram. (a) Measured $Q_{aq}$ (in m³/s) vs $Q_{oil}/Q_{aq}$. Stable jets were observed at flow rates above the symbols, which represent the lower boundary of the jetting region. Data for three concentrations of polyacrylamide are shown: 0.01 (○), 0.10 (■), and 1.0 wt % (▲). (b) Stability diagram plotted in units of the capillary number of the aqueous phase ($Ca \equiv \eta U/\sigma$) and the ratio of the flow rates, $Q_{oil}/Q_{aq}$. The line shows the prediction of our scaling analysis for the 1.0 wt % data with no adjustable parameters.

by the syringe pumps.) The shape of the jet also changed with flow rate: as $Q_{oil}$ increased, the base of the jet developed a flange owing to the small but nonnegligible inertia of the oil phase, which resulted in a low-pressure region downstream of the termination of the upstream capillary. Correspondingly, we note that in Figure 4 the Reynolds number of the oil $Re \equiv \rho_{oil} UR/\eta$, where $R = 250$ $\mu$m is the radius of the capillary in the gap region, increased from approximately 0.1 to 1 as the flange developed. Finally, the steady-state morphology was hysteretic: close to the limit of stability, stable jets existed only for decreasing and not increasing flow rates. As the critical stability limit was approached from above, we observed a series of rapid oscillations that propagated across the jet's surface, eventually resulting in a transition to dripping (droplet production). Apparently, high rates of shear and extension are needed to stabilize the jet as it crosses the gap.

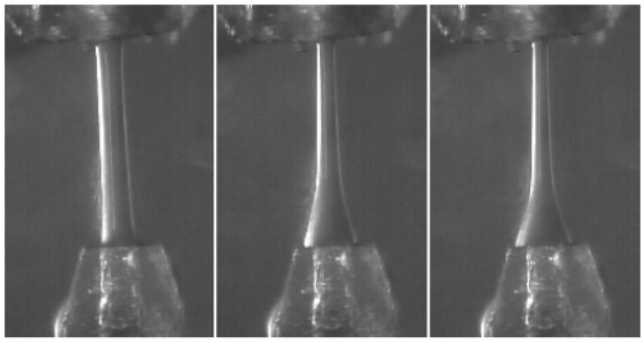

**Figure 4.** Images of a jet with a 1.0 wt % aqueous polymer solution with fixed $Q_{aq} = 50$ $\mu$L/min and $Q_{oil}$ increasing from 50 (at left) to 500 $\mu$L/min (at right). The direction of the flow is from bottom to top.

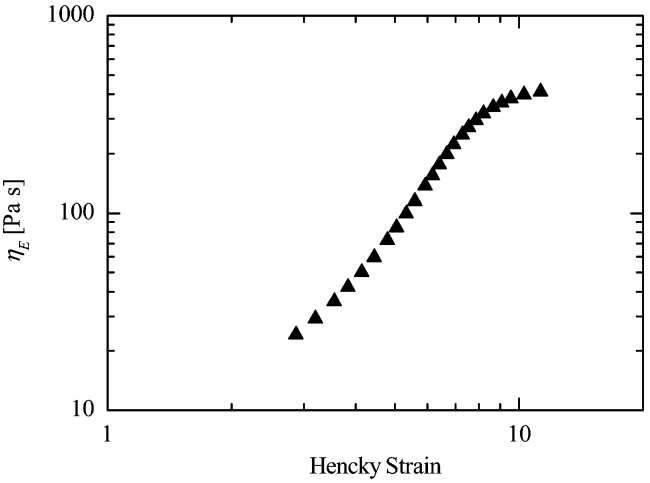


**Figure 5.** Measured transient uniaxial extensional viscosity, $\eta_E$, of 1.0 wt % PAA in water (▲) as a function of Hencky strain at a Deborah number $De = 2/3$.

Motivated by our observations, we wish to identify the causes of stable jet formation during the hydrodynamic flow focusing of a viscoelastic fluid. Within a stable fluid jet the Laplace pressure arising from surface tension must be balanced by the flow-induced viscous and elastic stresses within the fluid filament (jet) and by inertial stresses. However, because of the low Reynolds number, inertial stresses can be neglected. To quantify this force balance, we estimate the net stress acting on a disc-shaped slice of the aqueous jet. The surface tension leads to a stress given by $T_\sigma = 2\sigma/R_{aq,u}$, where $R_{aq,u}$ is the radius of the aqueous phase in the upstream region, which we will equate to the inner radius of the upstream capillary $R_{cap,u}$. The surface tension was assumed to be $\sigma = 54$ mN/m. The radius of curvature of the fluid filament in the axial direction is significantly larger than in the radial direction, and its contribution to the stress can be neglected. The hoop stresses generated by surface tension are destabilizing and will drive the fluid filament to pinch off into drops.

The shear stress exerted on the inner aqueous phase by the oil phase, on the other hand, tends to stabilize the jet by suppressing fluctuations along the interface. The shear stress can be approximated as $T_S = \eta_{aq}\dot{\gamma} \approx \eta_{aq}Q_{aq}/\pi R_{cap,u}^3$. In this low capillary number regime, $Ca \equiv \eta U/\sigma < 10^{-2}$, the surface stresses dominate the shear stresses, $T_\sigma \gg T_S$. Consequently, we can neglect the shear stresses.

Because the inner phase is viscoelastic, elastic stresses must also be considered in the force balance. A normal stress equal to $T_N = \Psi_1\dot{\gamma}^2$ is generated inside the polymer solution in the shear flow upstream of the flow focusing. Here, $\Psi_1$ is the first normal stress coefficient taken from the shear rheology measurements, and $\dot{\gamma} = 4Q_{aq}/(\pi R_{aq,u}^3)$ is the shear rate along the wall of the upstream capillary estimated from the laminar-flow (Poiseuille) solution of a Newtonian fluid in a pipe. Although this expression does not account for shear-dependent viscosity, it is a good first approximation.[47] Finally, we consider the extensional stress, $T_E = \eta_E\dot{\epsilon}$, produced in the filament as it necks down under an extensional flow, where $\dot{\epsilon}$ is the rate of extension. The extensional Hencky strain that accumulates in the fluid filament as it is accelerates into the downstream capillary is $\epsilon = 2\ln(R_{aq,u}/R_{aq,d})$, where $R_{aq,d}$ is the downstream radius of the aqueous solution.[48] The value of $R_{aq,d}$ can be measured, but for simplicity we assume that the flow in the downstream tubing is Poiseuille and find

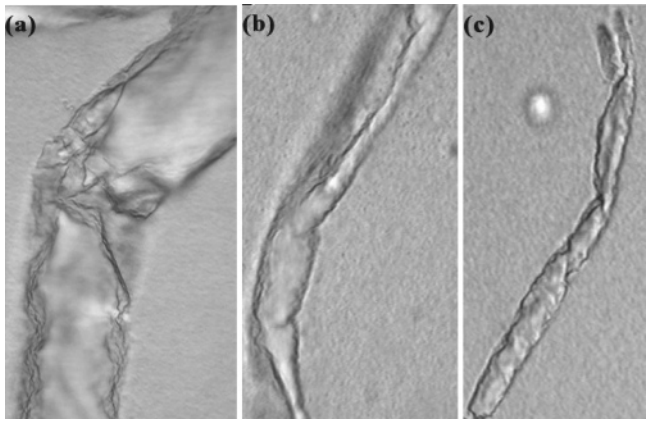


**Figure 6.** Images of hollow elastic tubes formed by aggregation of colloidal PMMA spheres on the surface of a stabilized jet (brightfield optical microscopy). The tubes are approximately 90 $\mu$m in diameter and suspended in hexadecane; no aqueous phase remains.

$$\frac{Q_{oil}}{Q_{aq} + Q_{oil}} = \frac{[1 - 2(R_{cap,d}/R_{aq,d})^2 + (R_{cap,d}/R_{aq,d})^4]}{[(\eta_{aq} - \eta_{oil})/\eta_{oil} + (R_{cap,d}/R_{aq,d})^4]} \quad (1)$$

where $R_{cap,d}$ is the known inner radius of the downstream capillary. Assuming a uniform extension rate within the flow-focusing region of length $L$, we define $\dot{\epsilon} = \epsilon/\tau_{res}$, where $\tau_{res}$ is the typical time it takes for the fluid to travel across the flow-focusing region, $\tau_{res} = \pi L R_{cap,u}^2/Q_{aq}$.

Capillary breakup rheometry measurements[49,50] of the three solutions were performed using a filament stretching rheometer.[41,51] A plot of the extensional viscosity, $\eta_E$, as a function of Hencky strain, $\epsilon = \dot{\epsilon}t = -2\ln(R_{mid}(t)/R_0)$, is shown for the 1.0 wt % PAA solution in Figure 5. Here $R_{mid}$ is the midpoint radius of the fluid filament and $R_0$ is the initial midpoint radius. The measurements were performed at $De = 2/3$. The 1.0 wt % PAA solution shows significant strain hardening with increasing strain, approaching an equilibrium value of $\eta_E = 420$ Pa·s or $Tr = 140$ at large Hencky strains. The extensional viscosities of the more dilute solutions were not measurable because of their low shear viscosities and short relaxation times. Nonetheless, we expect that even though their extensional viscosities would be signifi-

(47) Bird, R. B.; Armstrong, R. C.; Hassager, O. *Dynamics of Polymeric Liquids*; John Wiley & Sons: New York, 1987; Vol. 1 (Fluid Mechanics).
(48) Rothstein, J. P.; McKinley, G. H. *J. Non-Newtonian Fluid Mech.* **1999**, *86*, 61−88.
(49) Rodd, L. E.; Scott, T. P.; Cooper-White, J. J.; McKinley, G. H. *Appl. Rheol.* **2005**, *15*, 12−27.
(50) Anna, S. L.; McKinley, G. H. *J. Rheol.* **2001**, *45*, 115−138.
(51) Rothstein, J. P.; McKinley, G. H. *J. Rheol.* **2002**, *46*, 1419.

cantly smaller than in the 1.0 wt % PAA solution, their equilibrium Trouton ratios would be significantly larger.[51]

By looking at the relative magnitude of the forces acting on the fluid jets we can infer much of their behavior. When $T_\sigma > T_N + T_E$, the jet will pinch off into droplets. When $T_\sigma < T_N + T_E$, the drops will extend into the downstream capillary and form jets. The transition from dripping to jetting can then be reasonably approximated by balancing the stresses such that $T_\sigma = T_N + T_E$. As seen in Figure 3b, the scaling analysis for the 1.0 wt % PAA solution has the right form, qualitatively agreeing with our experimental measurements with no adjustable parameters. The scaling analysis does, however, underestimate the critical flow rate by a factor of about two. Although the agreement between our scaling analysis and the experimental measurements is reasonably good, a full linear stability analysis is required to precisely pinpoint the critical flow rate for the dripping-to-jetting transition for viscoelastic fluids.

The stability of the liquid jets can be enhanced through changes to several geometric and rheological parameters. According to our scaling analysis, setting $Q_{oil}/Q_{aq} = 10$, $R_{cap,d} = 50\ \mu$m, and $L = 650\ \mu$m, the critical $Q_{aq}$ decreases by a factor of 10 if $R_{cap,u}/R_{cap,d}$ is reduced by a factor of 3 or by 100 if this ratio is reduced by a factor of 7. In experiments with a smaller upstream capillary ($R_{cap,u} = 10\ \mu$m), we observed a dramatic reduction of the minimum $Q_{aq}$, but quantitative measurements of the volume flow rate were not accessible at such low flow rates.

Once the fluid jet has been formed, it will remain coherent in the downstream capillary—despite the absence of extensional flow—for a time on the order of the viscoelastic-capillary time $\tau_E$. For the 1 wt % PAA solution, $\tau_E = 0.4$ s. At flow rates corresponding to the transition from periodic dripping to stable jetting, this corresponds to a stable thread of length 1 mm. However, recent studies have also shown that hydrodynamic confinement can dramatically slow the break-up of liquid jets when the radius of the jet approaches the radius of the confining tube.[34−36] For a ratio of $\Lambda = R_{cap,d}/R_{aq,d} = 2$, lattice−Boltzmann simulations[35] show an approximately 3-fold reduction of the rate at which capillary undulations grow along a confined filament. Thus, combination of viscoelastic and confinement effects can keep the jets stable long enough that they can serve as ideal templates for materials fabrication.

To form hollow elastic tubes using the cylindrical liquid interface as a template, colloidal poly(methyl methacrylate) (PMMA) spheres were suspended in hexadecane (exterior phase) at a concentration of 0.1 vol %. The sphere diameter was approximately 0.4 $\mu$m, and spheres were sterically stabilized by poly(hydroxystearic acid) and labeled with NBD fluorescent dye (7-chloro-4-nitrobenzofurazan).[52] An aqueous solution of PAA ($c_p = 1.0$ wt %) was used as the interior phase. We recovered large numbers (at least on the order of 100) of coated cylinders by draining the flow device into a vial. The aqueous phase departed from these structures, leaving a continuous hexadecane fluid with no oil−water interface. Figure 6 shows images of three representative elastic cylinders. We found, as expected from previous experiments,[53,54] that the PMMA particles had adsorbed strongly at the hexadecane−water interface during the 1−10 s required for a segment of the jet to travel through the device. Earlier investigations found single layers of particles, and our images are consistent with this, though we were unable to resolve individual particles to verify the number of layers. The collected hollow tubes were tough, clearly able to maintain their shape even as the water escaped and after having been bent through an angle of at least 30° (as in Figure 6a). This toughness suggests that the particles aggregated or were jammed at the interface and formed a two-dimensional solid[55] whose critical stress exceeded the hexadecane−water surface tension. We anticipate that longer cylindrical shells can be produced using an optimized collection geometry, since in our case the shells were forced into an abrupt turn in the outflow, which might have broken or severely bent them.

In summary, we have shown that stable fluid jets with a diameter of 4−90 $\mu$m and length of at least 2 cm are readily formed by hydrodynamic focusing of a viscoelastic solution of polyacrylamide in water with immiscible hexadecane. The measured stability diagrams agree qualitatively with the model presented here, and the results may be useful more generally, for example, in predicting the behavior of non-Newtonian fluids in microfluidic devices. Finally, we demonstrated that stable jets serve as templates for fabrication of hollow, semipermeable elastic tubes with potential applications in encapsulation and as lightweight additives to enhance the toughness of materials.

**Acknowledgment.** We thank Erik Miller and Avinash Bhardwaj for the rheological measurements. A.D.D. and K.V.E. gratefully acknowledge support from Kraft Foods, Inc. through their NanoteK program as well as a University of Massachusetts Faculty Research Grant. J.P.R. acknowledges support from 3M through their Non-tenured Faculty Award Program and the National Science Foundation through grant no. CTS-0421043.

LA0614987

(52) Jardine, R. S.; Bartlett, P. *Colloids Surf. A: Physicochem. Eng. Asp.* **2002**, *211*, 127−132.

(53) Nikolaides, M. G.; Bausch, A. R.; Hsu, M. F.; Dinsmore, A. D.; Brenner, M. P.; Gay, C.; Weitz, D. A. *Nature (London)* **2002**, *420*, 299−301.

(54) Hsu, M. F.; Nikolaides, M. G.; Dinsmore, A. D.; Bausch, A. R.; Gordon, V. D.; Chen, X.; Hutchinson, J. W.; Weitz, D. A. *Langmuir* **2005**, *21*, 2963−2970.

(55) Vella, D.; Aussillous, P.; Mahadevan, L. *Europhys. Lett.* **2004**, *68*, 212−218.